Evolution of collectivity and evidence of octupole correlations in ^{73}Br

S. Bhattacharya,[1] T. Trivedi,[1,*] D. Negi,[2] R. P. Singh,[3] S. Muralithar,[3] R. Palit,[4] I. Ragnarsson,[5] S. Nag,[6] S. Rajbanshi,[7] M. Kumar Raju,[8] V. V. Parkar,[9] G. Mohanto,[9] S. Kumar,[10] D. Choudhury,[11] R. Kumar,[3] R. K. Bhowmik,[3] S. C. Pancholi,[3] and A. K. Jain[12]

[1]*Department of Pure & Applied Physics, Guru Ghasidas Vishwavidyalaya, Koni, Bilaspur 495009, India*
[2]*UM-DAE Centre for Excellence in Basic Sciences, Mumbai 400098, India*
[3]*Inter University Accelerator Center, Aruna Asaf Ali Marg, New Delhi 110067, India*
[4]*Department of Nuclear and Atomic Physics, Tata Institute of Fundamental Research, Mumbai 400005, India*
[5]*Division of Mathematical Physics, LTH, Lund University, P.O. Box 118, SE-22100 Lund, Sweden*
[6]*Department of Physics, IIT (BHU), Varanasi 221005, India*
[7]*Department of Physics, Presidency University, Kolkata 700073, India*
[8]*Research Center for Nuclear Physics, Osaka University, Osaka 5670047, Japan*
[9]*Nuclear Physics Division, Bhabha Atomic Research Centre, Mumbai 400085, India*
[10]*Department of Physics and Astrophysics, University of Delhi, Delhi 110007, India*
[11]*Department of Physics, Indian Institute of Technology, Ropar, Punjab 140001, India*
[12]*Amity Institute of Nuclear Science & Technology, Amity University, Noida 201313, India*

(Received 1 April 2019; revised manuscript received 4 May 2019; published 22 July 2019)

High-spin states in the ^{73}Br nucleus have been populated via the ^{50}Cr(^{28}Si, αp)^{73}Br fusion evaporation reaction with a beam energy of 90 MeV. The deexciting gamma rays were detected using the Indian National Gamma Array (INGA). Using the γ-γ coincidence technique, two new bands and eight new interconnecting transitions have been added. The strong interconnecting $E1$ transitions, between positive and negative parity bands, ensure the existence of octupole correlations at low spin. Line shapes have been observed for 17 transitions, which were analyzed by the Doppler-shift attenuation method to determine the lifetime of excited states of the yrast negative parity band and its signature partner band along with the positive parity band. The deduced transitional quadrupole moments Q_t for the ground state band decrease with increasing spin, with their values ranging from 2.88 to 1.00 eb. A similar trend in the quadrupole moment has also been observed for the signature partner as well as for the positive parity band. This decrease in Q_t with increasing spin for these bands is interpreted in terms of the cranked Nilsson-Strutinsky model and total Routhian surface calculations, which indicate possible band termination at higher spin.

DOI: 10.1103/PhysRevC.100.014315

I. INTRODUCTION

Atomic nuclei are examples of extremely complicated finite quantum many-body systems. The nucleons inside the nucleus interact via nucleon-nucleon interactions, giving rise to a variety of shapes and phenomena. Experimental investigations at extreme excitation energy and angular momenta help us to improve our understanding of the interplay between single-particle and collective degrees of freedom which are responsible for the intriguing features exhibited by atomic nuclei. Particularly, one of the interesting phenomena is the occurrence of highly deformed rotational bands which terminate at high spins. In smoothly terminating bands, terminating states are generated when all the available valence particles in a specific configuration are aligned along the rotational axis. As a result the rotating nucleus at intermediate spin gradually loses its collectivity and terminates to a noncollective state at higher spins [1]. Experimentally, terminating bands were first observed in ^{158}Er [2] and subsequently in $A \approx 110$ as well as in $A \approx 70$ mass regions[1].

Nuclei in the $A \approx 70$ mass region are known to exhibit shape coexistence and shape evolution due to the alignment of protons and neutrons. These have been confirmed by recent lifetime measurements of high spin states in ^{74}Kr [3], ^{75}Kr [4],^{74}Se [5], ^{72}Se [6], etc. The yrast band of ^{72}Se exhibits a shape coexistence after $\hbar\omega = 0.4$ MeV [6]. Similarly, ^{73}As has revealed prolate-oblate shape coexistence between positive and negative parity bands at low spins [7]. Most of the odd-A Br isotopes exhibit signature inversion and signature splitting due to the occupation of valence particles in the $g_{9/2}$ orbitals. In particular, the ^{75}Br nucleus shows a change of triaxiality due to the alignment of neutron and proton distributions in a $\pi g_{9/2} \otimes \nu g_{9/2}$ configuration [8] and the ^{77}Br nucleus shows signature splitting as well as γ softness (change in triaxiality from $\gamma \approx +30^\circ$ to $\gamma \approx -30^\circ$) [9]. The ^{73}Br nucleus lies in between the well studied ^{72}Br [10,11] and ^{74}Br [12] nuclei. In ^{72}Br, six rotational bands including two

*Corresponding author: ttrivedi1@gmail.com

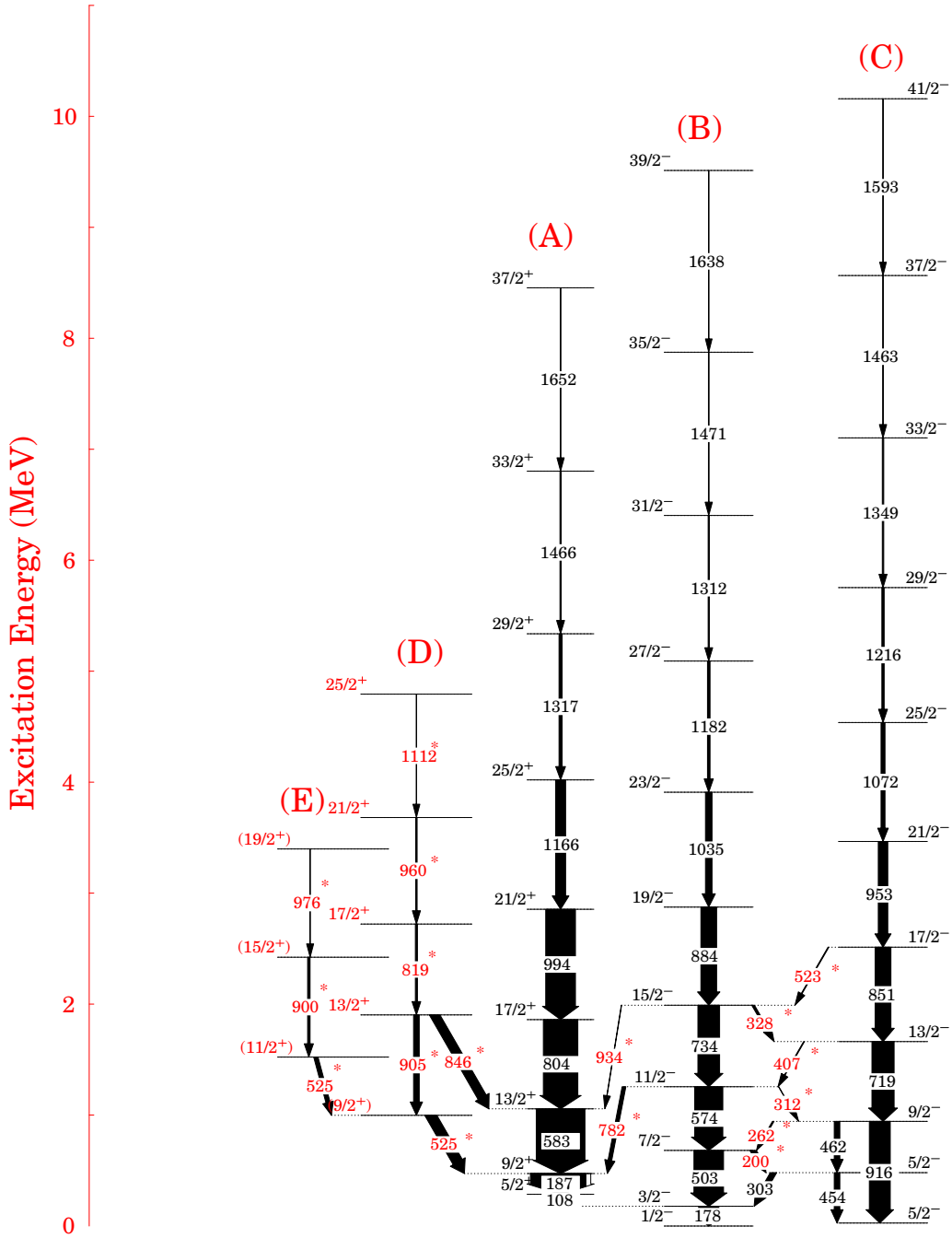

FIG. 1. Partial level scheme of ^{73}Br based on the present work and the previous study [13]. The newly observed transitions in the present work are marked by asterisks.

negative parity signature partner bands and one positive parity signature partner band have been observed. A similar band structure has been reported for ^{74}Br as well. However, in ^{73}Br only one negative parity band with its signature partner band along with only one signature of a positive parity band have been observed in previous studies [13]. In the present studies, we observed the missing positive parity signature partner band for the first time.

In particular, the ^{73}Br nucleus, with $Z = 35$ and $N = 38$, having valence protons and neutrons in positive parity intruder $g_{9/2}$ and normal parity $p_{3/2}$ orbitals with $\Delta l = 3$, $\Delta j = 3$, and $\Delta\pi = -1$, lying in the proximity of the Fermi surface, could lead to octupole correlations. Indeed, octupole correlations were recently observed in the ^{78}Br isotope [14]. Prior to the present work, high spin states in the ^{73}Br nucleus were investigated by Heese *et al.* [15] and Plettner *et al.* [13] using ^{40}Ca(^{36}Ar, $3p$)^{73}Br and ^{40}Ca(^{40}Ca, $\alpha 3p$)^{73}Br fusion evaporation reactions, respectively. Plettner *et al.* [13] observed three strong rotational bands up to very high rotational frequency and predicted they would be candidates for terminating bands. Heese *et al.* [15] performed lifetime measurements for these bands way back in 1987, long before Plettner's studies.

However, this lifetime information is quite insufficient to support Plettner's predictions as it is very limited and suffers from large uncertainties. Thus, it will be interesting to perform detailed gamma-ray spectroscopy with more precise lifetime measurements of high spin states in ^{73}Br to probe octupole correlations and band termination in a single nucleus. We have performed these measurements with the high efficiency Indian National Gamma Array (INGA) [16] with better statistics.

In the present work, two $\Delta I = 2$ positive parity bands consisting of nine new transitions have been identified and placed in the level scheme. In addition, two strong interconnecting $E1$ transitions linking the positive and negative parity bands have been identified. Further, six new interconnecting transitions have been placed in between the two negative parity bands. The directional correlation of oriented nuclei ratio, angular distribution from oriented nuclei, and integrated polarization directional correlation of oriented nuclei (IPDCO) ratio have been measured to assign the spin and parity of these states. In order to get better insight into the evolution of collectivity at high spins, lifetime measurements using the Doppler-shift attenuation method (DSAM) have been carried out. The properties of the rotational bands observed up to high spins are compared with the cranked Nilsson-Strutinsky model and total Routhian surface calculations.

II. EXPERIMENTAL DETAILS

High spin states in ^{73}Br were populated through the ^{50}Cr(^{28}Si, αp)^{73}Br reaction. A ^{28}Si beam of 90 MeV energy, provided by the 15UD Pelletron accelerator at IUAC, New Delhi was bombarded on a ^{50}Cr target of thickness 550 μg/cm^2 backed with 12 mg/cm^2 gold. The recoiling nuclei were stopped in the backing and the recoil velocity of ^{73}Br was about 2.5% of the velocity of light. The deexciting γ rays were detected using 17 Compton-suppressed clover detectors during the experiment. A total of 9×10^8 γ-γ coincidence events were collected in event-by-event mode. The detectors were placed at five different angles of 32° (two clovers), 57° (four clovers), 90° (five clovers), 123° (two clovers), and 148° (four clovers). After calibration and gain matching of individual crystals, add-back spectra were generated for all the clovers and the coincidence data were stored in a γ-γ matrix. The RADWARE software package [17] was used for the analysis of the matrix. This γ-γ coincidence matrix was used to find new γ-ray transitions placed in the level scheme. The multipolarities of the γ-ray transitions were assigned based on directional correlation of oriented nuclei ratio (DCO ratio) measurements and angular distribution from oriented nuclei (ADO) ratio measurements. For DCO measurements, an asymmetric matrix consisting of events detected by the clover detectors at 148° on one axis and at 90° on the other axis was constructed. Similarly, for ADO measurements, 32° and 90° angle dependent matrices were made and intensities of transition were compared for the two angles. However, for the application of the Doppler-shift attenuation method, the angle dependent matrices were built by taking events in the 148° or 32° detectors along one axis and all other detectors along the second axis. The line-shape spectra were created from the background subtracted spectra using these matrices.

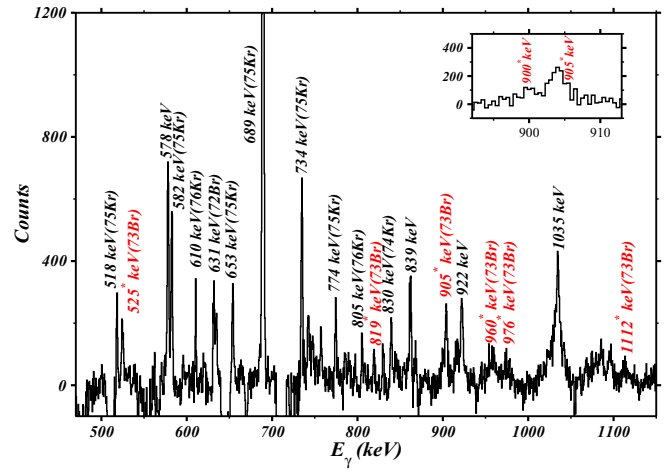

FIG. 2. Double-coincidence gated spectrum of 187 and 525 keV transitions, indicating the quadrupole transitions of bands D and E.

III. DATA ANALYSIS AND RESULTS

A. Level scheme

The partial level scheme of ^{73}Br obtained from the present work along with the previous results [13] is shown in Fig. 1. In the previous work, Plettner *et al.* [13] reported the yrast negative parity band with its signature partner band up to spin $65/2\,\hbar$. However, from our data it has been confirmed up to spin $41/2\,\hbar$ at an excitation energy of 10.158 MeV. In addition, two new $\Delta I = 2$ positive parity bands (labeled as D and E), consisting of nine new transitions have been identified and placed in the level scheme. The new transitions are labeled in red and marked with an asterisk, as shown in Fig. 1. The positive parity band D, consisting of four new γ-ray transitions with energies 905, 819, 960, and 1112 keV, has been observed up to $25/2^+$ with an excitation energy of 4.793 MeV. The coincident gate on the 525 and 187 keV transitions has been used to identify these transitions. A new positive parity band E has been identified and observed up to $19/2^+$ with an excitation energy of 3.399 MeV. Two new γ-ray transitions with energies of 900 and 976 keV have been placed in cascade above the $11/2^+$ state. The representative spectrum of the 525 and 187 keV coincident gate confirming band D and E is displayed in Fig. 2. Similarly, six new interconnecting transitions (200, 262, 312, 328, 407, and 523 keV) have been identified and placed in between the two negative parity bands B and C. In addition, two new interconnecting transitions (782, 934 keV) have been placed in between the positive parity band A and the negative parity band B. The representative spectrum confirming these transitions from the coincident gate on 187 and 884 keV is shown in Fig. 3. The relative intensities in the positive parity band A have been determined up to the $37/2^+$ state using the 187, 583, and 804 keV transition gates. However, for the yrast negative parity band B and its signature partner band C, the γ-ray intensities have been determined up to the $39/2^-$ and $41/2^-$ states respectively. Similarly, the intensities of band D and E were extracted using the 187, 525, and 905 keV transitions. The relative intensities of various transitions are listed in Table I.

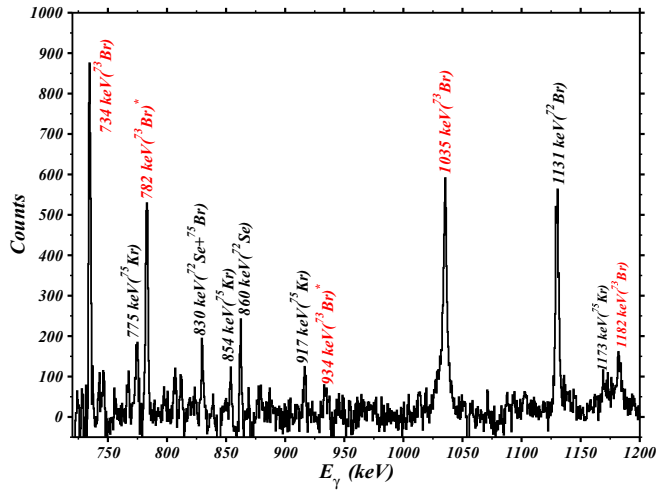

FIG. 3. Double-coincidence gated spectrum of 187 and 884 keV transitions indicating 782 and 934 keV interconnecting transitions marked by asterisks.

B. Angular correlation and polarization measurements

The spin and parity of different states were assigned by directional correlation of oriented states (DCO) and integrated polarization directional correlation from oriented nuclei (IPDCO) methods. The DCO ratio for the present geometry is defined as

$$R_{DCO} = \frac{I\gamma_1 \text{ observed at } 148^\circ \text{ gated on } \gamma_2 \text{ at } 90^\circ}{I\gamma_1 \text{ observed at } 90^\circ \text{ gated on } \gamma_2 \text{ at } 148^\circ}, \quad (1)$$

where $I\gamma$ represents the intensity of the γ rays. When the gate is on a stretched quadrupole transition, the R_{DCO} value is $\approx$1.0 for a stretched quadrupole transition and $\approx$0.5 for a stretched dipole transition. Similarly, the gate on a stretched dipole transition gives $R_{DCO} \approx 2.0$ for a quadrupole transition and $\approx$1.0 for a pure dipole transition. However, the R_{DCO} value could not be determined precisely for comparatively weak transitions or due to the unavailability of pure gating transitions. In order to overcome this deficiency, an alternative method was adopted to determine the multipolarities of γ rays using the angular distribution from oriented nuclei (ADO) ratios method [18]. The ADO ratio for γ transitions is defined as

$$R_\theta = \frac{I\gamma_1 \text{ observed at } 32^\circ \text{ gated on } \gamma_2 \text{ at all angles}}{I\gamma_1 \text{ observed at } 90^\circ \text{ gated on } \gamma_2 \text{ at all angles}}. \quad (2)$$

For the present measurement, typical values of the ADO ratios have been found for stretched dipole and quadrupole transitions as 0.9 and 1.9 respectively. The DCO and ADO ratios for the positive parity band A have been determined up to the $29/2^+$state using the 108 and 804 keV gates as the 187 and 583 keV transitions also belong to the ^{75}Kr nucleus, which was populated with a comparatively high cross section. For the yrast negative parity band B, DCO and ADO values are calculated up to the $27/2^-$ state using 503 and 574 keV gate. DCO and ADO values for its signature partner band C were determined up to the $25/2^-$ state. Similarly, the multipolarities have been assigned for the two newly identified positive parity bands using 187, 525, and 905 keV gating transitions. The DCO and ADO values of the interconnecting 782 keV transition were found to be 0.75 and 0.96, as a result of which $E1$ multipolarity was assigned to the transition (see Table I).

The parities of some of the states were assigned by measuring the polarization asymmetry using the clover detectors at 90° which act as a Compton polarimeter. The polarization asymmetry $\triangle$ for a γ-ray transition is defined as in Ref. [19]:

$$\triangle = \frac{a(E_\gamma)N_\perp - N_\parallel}{a(E_\gamma)N_\perp + N_\parallel}, \quad (3)$$

where $N_\perp$ ($N_\parallel$) is the count of γ-ray transitions scattered perpendicular (parallel) to the reaction plane. The correction factor $a(E_\gamma)$ is a measure of the perpendicular-to-parallel scattering asymmetry within the crystals of the clover. In the present experiment, $a(E_\gamma)$ as a function of energy was measured as 0.98(2) using decay data of a ^{152}Eu radioactive source. For linear polarization measurements, two asymmetric matrices were constructed with coincidence events corresponding to parallel and perpendicular segments of the clover detectors (with respect to the emission plane) along one axis and coincident events corresponding to all the detectors of the array on the other axis [20]. A positive value of the IPDCO ratio indicates an electric nature of the transition while a negative value indicates the magnetic nature of the transition. The measured value of IPDCO for the 583, 804, 994, 1165, 574, 735, 884, 1035, 1182, 719, 851, 952, and 1172 keV transitions was found to be positive, whereas for the 846 and 407 keV transitions it is negative, showing their electric and magnetic nature, respectively (shown in Fig. 4).

In the present work, two positive parity quadrupole bands, D and E, have been identified for the first time in the ^{73}Br nucleus. They have been observed up to spin-parity $I^\pi = 25/2^+$ and $19/2^+$, respectively. The spin and parity of these bands have been measured using DCO ratio, ADO ratio, and IPDCO measurements. Based on systematic studies of the ^{70}As [21] and ^{73}As nuclei [7], the structure is indicative of a coupled rotational sequence with pronounced signature splitting. The structure of band D is of $\alpha = 0$ signature while band E has an $\alpha = 1$ signature.

C. Lifetime measurements

We measured the lifetimes of the excited states of positive and negative parity bands in ^{73}Br using the LINESHAPE program developed by Wells and Johnson [22]. The Monte Carlo simulation technique is used in this program for the velocity and directional history of a series of recoiling nuclei in the target and in the backing with a time step of 0.01 ps for 10 000 histories of energy losses at different depths. For the energy-loss calculations, shell corrected Northcliffe and Schilling [23] electronic stopping powers were used. Velocity profiles for different angles were generated using the geometry of the detectors as well as the array as input parameters [24]. The side-feeding intensities, extracted by using the intensity balance for each level of the cascade from the intensity of the transition and measured from present data, are shown in Table I. By assuming 100% side feeding into the top of the band, an effective lifetime of the top-most

TABLE I. Gamma ray transition energies ($E\gamma$), spin-parity assignments for the initial (I_i^π) and final (I_f^π) states, relative intensities ($I\gamma$), DCO ratios (R_{DCO}), ADO ratios (R_θ), multipolarities, and parent-state excitation energies (E_i) associated with the γ rays observed from the high-spin decay of ^{73}Br.

E_i (keV)	$(I_i^\pi) \rightarrow (I_f^\pi)$	E_γ (keV)[a]	I_γ	R_{DCO}	R_θ	IPDCO	Assignment
178.1	$3/2^- \rightarrow 1/2^-$	178.1	35.5(10)	0.80(11)	0.75(10)		$E2/M1$
285.9	$5/2^+ \rightarrow 3/2^-$	107.8	13.4(11)	0.90(16)	1.30(12)		$E2/M1$
472.9	$9/2^+ \rightarrow 5/2^+$	187.0	100(10)	1.07(15)	2.05(10)		$E2$
1056.1	$13/2^+ \rightarrow 9/2^+$	583.2	87.6(5)	0.97(8)	2.16(5)	0.14(9)	$E2$
1860.1	$17/2^+ \rightarrow 13/2^+$	804.0	62.1(5)	1.01(7)	1.84(5)	0.20(9)	$E2$
2854.6	$21/2^+ \rightarrow 17/2^+$	994.5	53.5(5)	1.05(10)	1.99(5)	0.19(11)	$E2$
4020.4	$25/2^+ \rightarrow 21/2^+$	1165.8	18.1(10)	1.18(18)	1.97(10)		$E2$
5337.2	$29/2^+ \rightarrow 25/2^+$	1316.8	5.6(11)	0.80(20)	2.20(12)		$E2$
6803.2	$33/2^+ \rightarrow 29/2^+$	1466.0	2.2(13)				
8455.2	$37/2^+ \rightarrow 33/2^+$	1652.0	1.1(15)				
1255.3	$11/2^- \rightarrow 9/2^+$	782.4	6.6(5)	0.75(7)	0.96(5)		$E1$
1989.8	$15/2^- \rightarrow 13/2^+$	933.6	0.6(6)				
681.4	$7/2^- \rightarrow 3/2^-$	503.3	57.2(5)	0.87(7)	1.88(5)	0.05(11)	$E2$
1255.3	$11/2^- \rightarrow 7/2^-$	573.9	50.6(5)	1.02(7)	2.20(5)	0.14(12)	$E2$
1989.8	$15/2^- \rightarrow 11/2^-$	734.5	39.1(6)	1.08(7)	1.71(5)	0.18(10)	$E2$
2874.1	$19/2^- \rightarrow 15/2^-$	884.3	28.3(6)	1.14(8)	1.80(6)	0.33(11)	$E2$
3909.3	$23/2^- \rightarrow 19/2^-$	1035.2	11.8(11)	1.17(16)	1.99(11)	0.17(16)	$E2$
5091.4	$27/2^- \rightarrow 23/2^-$	1182.1	4.6(14)	0.91(13)	1.82(11)		$E2$
6403.4	$31/2^- \rightarrow 27/2^-$	1312.0	2.2(16)				
7874.4	$35/2^- \rightarrow 31/2^-$	1471.0	1.1(18)				
9512.4	$39/2^- \rightarrow 35/2^-$	1638.0	<1				
481.1	$5/2^- \rightarrow 3/2^-$	302.9	15.9(6)	0.8(16)	1.91(6)	0.06(12)	$E2/M1$
943.2	$9/2^- \rightarrow 5/2^-$	462.2	7.5(5)	1.07(10)	1.96(5)	0.07(8)	$E2$
943.2	$9/2^- \rightarrow 5/2^-$	916.2	37.7(5)	0.93(8)	1.96(5)	0.19(6)	$E2$
1662.1	$13/2^- \rightarrow 9/2^-$	718.9	39.9(5)	1.26(11)	1.76(5)	0.18(14)	$E2/M1$
481.1	$5/2^- \rightarrow 5/2^-$	454.1	5.9(5)	1.25(9)	2.35(6)	0.06(17)	$\Delta I = 0, E2/M1$
2512.9	$17/2^- \rightarrow 13/2^-$	850.8	28.5(5)	1.00(7)	1.78(6)	0.1(18)	$E2$
3465.5	$21/2^- \rightarrow 17/2^-$	952.6	17.1(5)	1.13(9)	1.81(6)	0.25(14)	$E2$
4537.4	$25/2^- \rightarrow 21/2^-$	1071.9	7.1(10)	1.01(20)	1.82(15)	0.15(19)	$E2$
5753.3	$29/2^- \rightarrow 25/2^-$	1215.9	4.1(11)		1.72(10)		$E2$
7100.3	$33/2^- \rightarrow 29/2^-$	1347.0	2.6(11)				
8563.3	$37/2^- \rightarrow 33/2^-$	1463.0	1.12(15)				
10156.3	$41/2^- \rightarrow 37/2^-$	1593.0	<0.5				
681.4	$7/2^- \rightarrow 5/2^-$	199.8	1.2(11)				
943.2	$9/2^- \rightarrow 7/2^-$	261.7	2.4(7)				
1255.3	$11/2^- \rightarrow 9/2^-$	312.1	0.5(6)				
1662.1	$13/2^- \rightarrow 11/2^-$	406.8	1.4(6)	0.62(12)	0.91(5)	−0.19(25)	$M1$
1989.8	$15/2^- \rightarrow 13/2^-$	327.7	1.32(7)				
2512.9	$17/2^- \rightarrow 15/2^-$	523.1	1.4(6)	0.46(12)	0.75(5)		$M1$
1902.6	$13/2^+ \rightarrow 9/2^+$	905.0	10.2(5)	1.4(18)	2.16(5)	0.28(17)	$E2$
2721.3	$17/2^+ \rightarrow 13/2^+$	818.7	3.7(6)	1.26(19)	1.99(5)		$E2/M1$
2422.4	$(15/2^+) \rightarrow (11/2^+)$	900.0	4.4(6)	1.00(6)	1.77(6)	0.31(15)	$E2$
1902.6	$13/2^+ \rightarrow 13/2^+$	846.5	16.6(7)	1.85(16)	2.42(5)	−0.20(19)	$\Delta I = 0, E2/M1$
997.6	$(9/2^+) \rightarrow (9/2^+)$	524.7	19.0(6)	1.70(8)	2.44(5)		$\Delta I = 0, E2/M1$
1522.5	$(11/2^+) \rightarrow (9/2^+)$	524.9	7.5(6)				
3681.3	$21/2^+ \rightarrow 17/2^+$	960.0	2.5(6)				
4793.3	$25/2^+ \rightarrow 21/2^+$	1112.0	0.5(13)				
3398.2	$(19/2^+) \rightarrow (15/2^+)$	975.7	0.6(6)				

[a]The uncertainties in the E_γ values lie between 0.5 and 1.3 keV, depending on the intensities.

state was estimated; this was then used as an input parameter to extract the lifetimes of lower states in the cascade. The LINESHAPE program [22] does a χ^2 minimization of the fit for (i) the transitional quadrupole moment Q_t for the level, (ii) the transitional quadrupole moment for the modeled side-feeding Q_{SF}, (iii) the factor to normalize the intensity of the fitted transition at each angle, (iv) the intercept and the slope of the background, (v) mean lifetime τ_{SF} if a cascade side-feeding

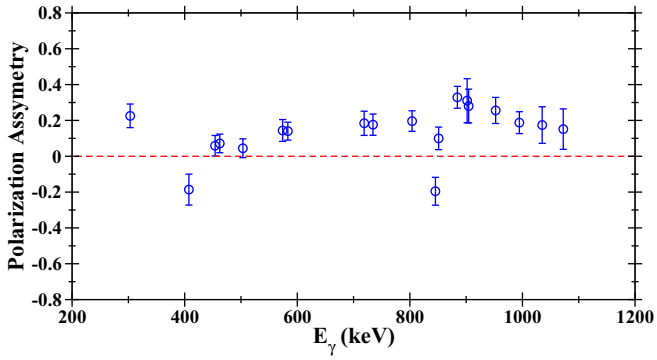

FIG. 4. Plot of polarization asymmetry for different γ transitions.

level is considered, and (vi) the intensity of contaminant peaks [25]. Once the χ^2 minimization was obtained by the MINUIT [26] program, the procedure was followed for the next lower level. After obtaining a χ^2 minimization for each level, a global fit was carried out. In the analysis, an effective lifetime was obtained for the topmost level by assuming a prompt feed to this level; for the rest of the transitions we used a rotational cascade side-feeding model of five transitions with a fixed moment of inertia of 19 $\hbar^2\,\mathrm{MeV}^{-1}$ throughout the analysis. Lifetimes were measured by analyzing separately the Doppler-broadened line shapes in 148° and 32° coincidence spectra, and the final lifetime values were obtained by taking averages of the results obtained from these two separate fits. Uncertainties in lifetimes were derived from the behavior of the χ^2 fit in the vicinity of the minimum [21,24]. The uncertainties quoted in the lifetimes do not include systematic errors due to the stopping power, which can be as large as 15%.

The lifetimes of the $17/2^+$ to $37/2^+$ levels in the positive parity band and from $17/2^-$ to $41/2^-$ levels in the negative parity bands were obtained by fitting the line shape at 148° and 32° (see Table II).

In positive parity band A, Doppler broadened line shapes were observed for 804, 994, 1166, 1317, and 1466 keV transitions above the $13/2^+$ state. The line shapes for the 804, 994, and 1166 keV transitions were obtained by putting a gate on the 583 keV transition; however, for the 1317 and 1466 keV transitions, an 804 keV gate was used to get clean line-shape spectra. The experimental and fitted line shapes for some representative transitions of band A at 148° and 32° are presented in Fig. 5. The lifetimes of the yrast negative parity band B and its signature partner band C were measured from states above $15/2^-$ to $41/2^-$ by gating below the transition of interest. The experimental and fitted line shapes at 148° and 32° for some representative transitions are shown in Fig. 6. The measured lifetimes for the 17/2 to 21/2 states in the positive and negative parity bands are found to be significantly smaller than the earlier reported values [15], which were derived from data with poorer statistics (see Table II).

TABLE II. Experimental lifetimes of excited states, transition strengths $B(E2)$, and transitional quadrupole moments Q_t for the positive and negative parity bands of ^{73}Br obtained in the present experiment. Excitation energies (E_x), gamma-ray energies (E_γ), and spins have been taken from Ref. [13].

Band	E_x (keV)	$(I_i^\pi) \rightarrow (I_f^\pi)$	E_γ (keV)	τ (ps) [15] previous	τ (ps) 148°	τ (ps) 32°	Adopted τ (ps)	Q_t (*e*b)	$B(E2)$ W.u.
Band A	1860.1	$17/2^+ \rightarrow 13/2^+$	804.0	1.5(3)	0.64(0.03)	0.62(0.03)	0.63(0.05)	$3.46^{+0.13}_{-0.12}$	213^{+18}_{-16}
	2854.6	$21/2^+ \rightarrow 17/2^+$	994.5	0.62(8)	$0.31^{+0.03}_{-0.02}$	0.32(0.01)	$0.32^{+0.03}_{-0.02}$	$2.83^{+0.14}_{-0.09}$	145^{+10}_{-12}
	4020.4	$25/2^+ \rightarrow 21/2^+$	1165.8	0.20(7)	$0.22^{+0.02}_{-0.10}$	$0.19^{+0.01}_{-0.02}$	$0.21^{+0.03}_{-0.10}$	$2.32^{+0.16}_{-0.39}$	99^{+90}_{-13}
	5337.2	$29/2^+ \rightarrow 25/2^+$	1316.8	0.16(7)	$0.11^{+0.03}_{-0.02}$	<0.32	$0.11^{+0.03}_{-0.02}$	$2.32^{+0.40}_{-0.20}$	103^{+23}_{-22}
	6803.2	$33/2^+ \rightarrow 29/2^+$	1466.0		<0.22		<0.22	>1.26	>30
Band B	1989.8	$15/2^- \rightarrow 11/2^-$	734.5	1.28(3)[a]				3.15(25)[a]	160^{+38}_{-16}[a]
	2874.1	$19/2^- \rightarrow 15/2^-$	884.3	0.85(10)	0.57(0.03)	$0.58^{+0.10}_{-0.07}$	$0.58^{+0.11}_{-0.08}$	$2.88^{+0.25}_{-0.22}$	144(23)
	3909.3	$23/2^- \rightarrow 19/2^-$	1035.2	0.37(7)	$0.32^{+0.02}_{-0.04}$	$0.29^{+0.03}_{-0.01}$	0.31(0.04)	$2.62^{+0.16}_{-0.15}$	122^{+18}_{-14}
	5091.4	$27/2^- \rightarrow 23/2^-$	1182.1	0.17(7)	0.13(0.01)	$0.17^{+0.02}_{-0.01}$	$0.15^{+0.02}_{-0.01}$	$2.67^{+0.15}_{-0.13}$	130^{+9}_{-15}
	6403.4	$31/2^- \rightarrow 27/2^-$	1312.0		0.15(0.01)	$0.15^{+0.02}_{-0.03}$	$0.15^{+0.02}_{-0.03}$	$2.04^{+0.12}_{-0.21}$	77^{+19}_{-9}
	7874.4	$35/2^- \rightarrow 31/2^-$	1471.0		0.13(0.04)	<0.21	0.13(0.04)	$1.62^{+0.32}_{-0.20}$	50^{+22}_{-12}
	9512.4	$39/2^- \rightarrow 35/2^-$	1638.0		<0.20		<0.20	>1.00	>19
Band C	2512.9	$17/2^- \rightarrow 13/2^-$	850.8	1.0(2)	$0.66^{+0.03}_{-0.01}$	$0.66^{+0.05}_{-0.03}$	$0.66^{+0.06}_{-0.05}$	$3.00^{+0.14}_{-0.10}$	145(12)
	3465.5	$21/2^- \rightarrow 17/2^-$	952.6	0.55(10)	0.35(0.01)	$0.30^{+0.03}_{-0.02}$	$0.33^{+0.03}_{-0.02}$	$3.14^{+0.18}_{-0.12}$	174^{+11}_{-15}
	4537.4	$25/2^- \rightarrow 21/2^-$	1071.9	0.40(8)	0.28(0.01)	0.18(0.01)	$0.23^{+0.01}_{-0.02}$	2.79(0.12)	139^{+14}_{-7}
	5753.3	$29/2^- \rightarrow 25/2^-$	1215.9		0.13(0.01)	$0.18^{+0.03}_{-0.06}$	$0.15^{+0.04}_{-0.07}$	$2.44^{+0.28}_{-0.33}$	113^{+99}_{-24}
	7100.3	$33/2^- \rightarrow 29/2^-$	1347.0		$0.20^{+0.04}_{-0.05}$	<0.26	$0.20^{+0.04}_{-0.05}$	$1.63^{+0.21}_{-0.19}$	50^{+17}_{-8}
	8563.3	$37/2^- \rightarrow 33/2^-$	1463.0		<0.24		<0.24	>1.22	>28

[a]Recoil distance measurement (RDM) technique [15].

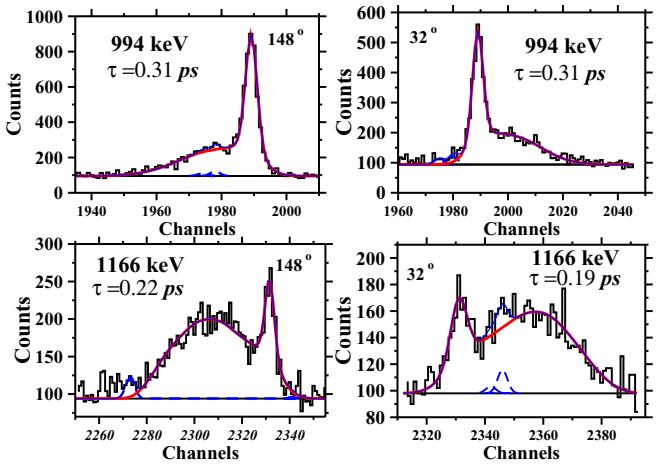

FIG. 5. Least-squares fit of line shapes of some representative transitions (994 and 1066 keV) for band A of ^{73}Br. The left-hand frames show the data for the 148° detectors and right-hand frames show the data for 32° detectors. The contaminant peaks are shown by blue color.

IV. DISCUSSION

A. Transitional quadrupole moment and transition strength

The reduced electric quadrupole transition probability $B(E2)$ and resulting transitional quadrupole moment Q_t obtained from the measured lifetimes are shown in Table II. The $B(E2)$ values are calculated from the measured lifetimes using the following relationship:

$$B(E2) = \frac{0.0816 B_r(E2)}{E_\gamma^5 \tau \times A^{4/3} \times 5.94 \times 10^{-6}[1+\alpha_t(E2)]} \text{ W.u.}, \quad (4)$$

where E_γ is the transition energy in MeV, τ is the partial lifetime of the transition (in ps) deduced from the fitted line

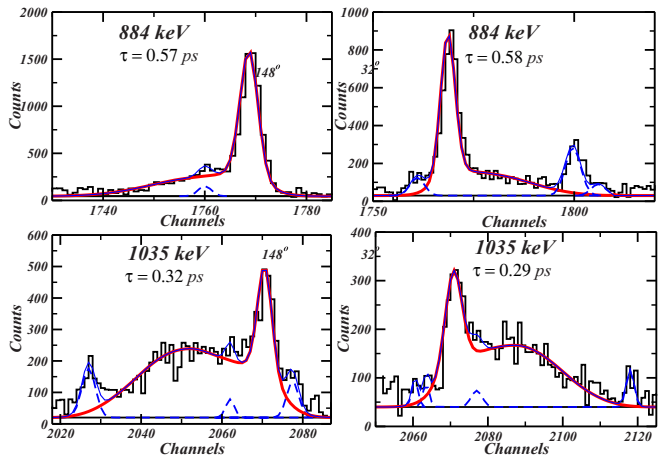

FIG. 6. Least-squares fits of line shapes of some representative transitions (884 and 1035 keV) for band B of ^{73}Br. The left-hand frames show the data for the 148° detectors and right-hand frames show the data for 32° detectors. The contaminant peaks are shown by blue color.

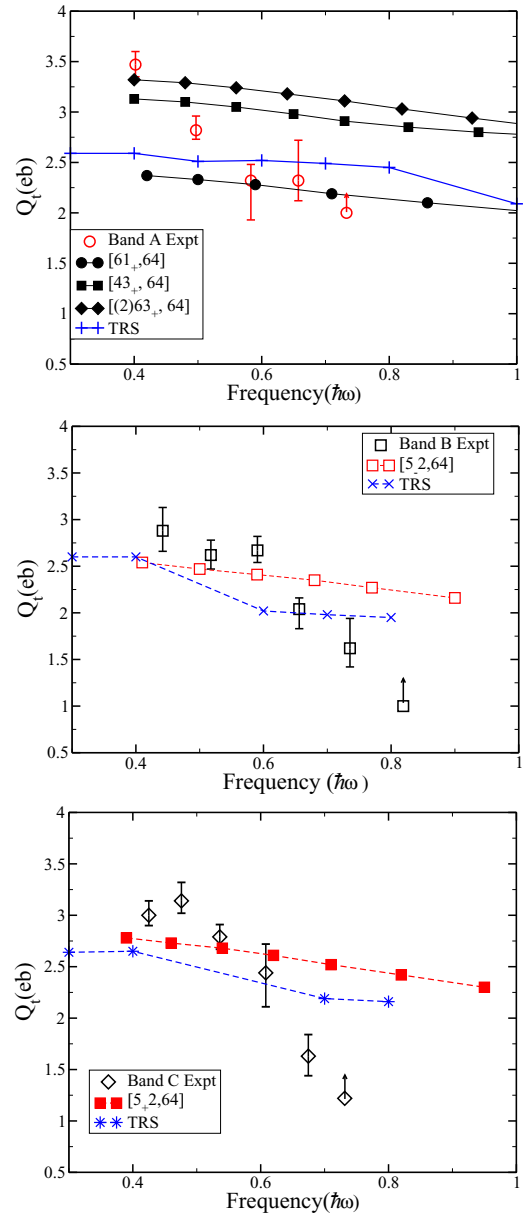

FIG. 7. The observed transitional quadrupole moments compared with those calculated in the CNS (labeled with configuration) and TRS formalisms.

shape of the state, α_t is the total internal conversion coefficient of the transition, and B_r is the branching ratio of the transition. The value of the transitional quadrupole moment Q_t was obtained from the $B(E2)$ using the rotational formula.

$$Q_t^2 = \frac{16\pi \times A^{3/4}}{29.7 \times 10^{-6}} \langle IK20|I-2K\rangle^{-2} B(E2, I \to I-2). \quad (5)$$

Here, $B(E2)$ is in Weisskopf units, Q_t is in eb and the term in angular brackets is a Clebsch-Gordon coefficient. For the angular momentum projection quantum number, the value $K = 3/2$ was used for the positive parity band and $K = 1/2$ for the negative parity bands. Figure 7 shows the variation of transitional quadrupole moment for the positive parity band A as a function of frequency from the present data. For

the positive parity band, the transitional quadrupole moment decreases from 3.46 eb at spin $17/2^+$ to 1.26 eb at spin $33/2^+$, showing a loss of collectivity with increasing spin and/or frequency.

The transitional quadrupole moment for the yrast negative parity band B is found to be decreasing from 2.88 to 1.00 eb and from 3.00 to 1.22 eb for its signature partner band C, as shown in Fig. 7. From the figures, it is evident that both the negative parity bands exhibit a similar trend of observed quadrupole moment, showing loss of collectivity with increasing spins. This loss in collectivity may be taken as a signature of terminating bands at high spin. However, this loss of collectivity is much more drastic than predicted.

B. Octupole correlation

Octupole correlations have been studied in more detail in $A \approx 220$ and ≈ 150 mass regions compared to nuclei lying in $A \approx 70$ mass region. However, the availability of an octupole driving pair of $g_{9/2}$ and $p_{3/2}$ proton orbitals in ^{73}Br at low excitation energy makes it an ideal case to exhibit octupole correlations. The experimental signatures of octupole correlations are enhanced $E1$ transition strength between opposite parity bands as well as the values of the $B(E1)/B(E2)$ ratio. Recently, octupole correlations have been reported in various isotopes of barium, cesium, and cerium. The average $B(E1)/B(E2)$ ratio in ^{124}Ba [27] is $\approx 0.04 \times 10^{-6}$ fm^{-2} and for ^{125}Ba [27] it is $\approx 0.035 \times 10^{-6}$ fm^{-2}. A similar $B(E1)/B(E2)$ ratio has been reported in ^{150}Ce [28], $\approx 0.04 \times 10^{-6}$ fm^{-2}, and in ^{152}Ce [29], $\approx 0.023 \times 10^{-6}$ fm^{-2}. However, in ^{73}Br, the extracted values of the $B(E1)/B(E2)$ ratio for the $11/2^-$ and $15/2^-$ states are 0.017×10^{-6} fm^{-2} and 0.004×10^{-6} fm^{-2}, respectively, which are comparable with ^{78}Br [14].

The $E1$ matrix elements between close-lying Nilsson orbitals are invariably small, which gives a transition strength $B(E1)$ value of the order of 10^{-6} Weisskopf unit [27]. However, in ^{73}Br the extracted values of the reduced transition probability $B(E1)$ are $0.46(9) \times 10^{-4}$ W.u. for the 782 keV transition and $0.64(6) \times 10^{-4}$ W.u. for the 933 keV transition, as shown in Table III. A similar enhancement in the $B(E1)$ strength has been reported for ^{125}Ba ($\approx 1.1 \times 10^{-4}$) [27], ^{124}Ba ($\approx 1.0 \times 10^{-4}$) [27] and ^{124}Cs ($\approx 1.85 \times 10^{-4}$) [30]. These $B(E1)$ values suggest comparatively weaker octupole correlations compared to nuclei lying in the 120 and 150 mass regions, which may be due to the interaction of lower j orbitals. Thus, the observed enhanced $B(E1)$ and $B(E1)/B(E2)$ ratios in ^{73}Br give evidences for octupole correlations in the $A \approx 70$ mass region, which will open a new territory of investigation of octupole correlations in this comparatively less studied mass region of the nuclear chart.

C. CNS calculations

In the previous work by Plettner *et al.* [13], the presently observed bands A, B, and C were observed up to high spin, $I \approx 65/2\,\hbar$. The authors discussed the origin of the bands in the framework of the configuration dependent cranked Nilsson-Strutinsky (CNS) model [1,31,32]. This is the model which is used in the present study, but with some modifications.

In the CNS model, the configurations are designated by the number of particles or holes in orbitals labeled by $\mathcal{N}$ shell and further grouped into high- and low-j shells. Signature $\alpha = 1/2$ or $-1/2$ is also a preserved quantum number, where the rotation breaks the signature degeneracy of the static potential. The calculations are performed with κ and μ parameters fitted for the $A = 80$ region [1]. These parameters define the strength of the ls and l^2 terms in the modified oscillator potential [33]. The total energy is calculated as a sum of the rotating liquid drop energy and the shell energy, using the Strutinsky shell correction formalism [34,35]. The static liquid drop reference used is the Lublin-Strasbourg drop (LSD) [36]. The rigid body moment of inertia is calculated with a radius parameter of $r_0 = 1.16$ fm and diffuseness of $a = 0.6$ fm [31]. The calculations minimize the total energy for the different configurations with respect to deformation, ε_2, ε_4, and γ, at different spins. The configurations are labeled as

$$[p_1 p_2, n_1 n_2],$$

where p_1 and n_1 correspond to the numbers of protons and neutrons in $p_{3/2}$, $f_{5/2}$ (pf) orbitals, respectively, whereas p_2 and n_2 are proton and neutron occupations in $g_{9/2}$ orbitals.

TABLE III. Calculated $B(E1)/B(E2)$ ratios, $B(E1)$, $B(E2)$, and $B(M1)$ values for the octupole band from the present experiment.

Nucleus	E_γ (keV)	$(I_i^\pi) \rightarrow (I_f^\pi)$	$\frac{B(E1)}{B(E2)}$ (10^{-6}fm^{-2})	$B(\sigma\lambda)$ (W.u.)
^{73}Br	781.9	$(11/2)^- \rightarrow (9/2)^+$	0.017(6)	$0.46(9) \times 10^{-4}$
	573.9	$(11/2)^- \rightarrow (7/2)^-$		168.3(12)[a]
	311.6	$(11/2)^- \rightarrow (9/2)^-$		0.003(6)
	933.3	$(15/2)^- \rightarrow (13/2)^+$	0.004(6)	$0.64(6) \times 10^{-4}$
	734.5	$(15/2)^- \rightarrow (11/2)^-$		160.01(25)[a]
	327.4	$(15/2)^- \rightarrow (13/2)^-$		0.002(6)
^{125}Ba [27]	475	$25/2^+ \rightarrow (23/2)^-$	0.05(1)	0.8×10^{-4}
	777	$23/2^+ \rightarrow (21/2)^-$	0.18(3)	3×10^{-4}
	807	$19/2^+ \rightarrow (17/2)^-$	0.07(2)	1×10^{-4}
	680	$15/2^+ \rightarrow (13/2)^-$	0.015(7)	0.15×10^{-4}
	631	$13/2^+ \rightarrow (11/2)^-$	0.027(8)	0.2×10^{-4}

[a]From Ref. [15].

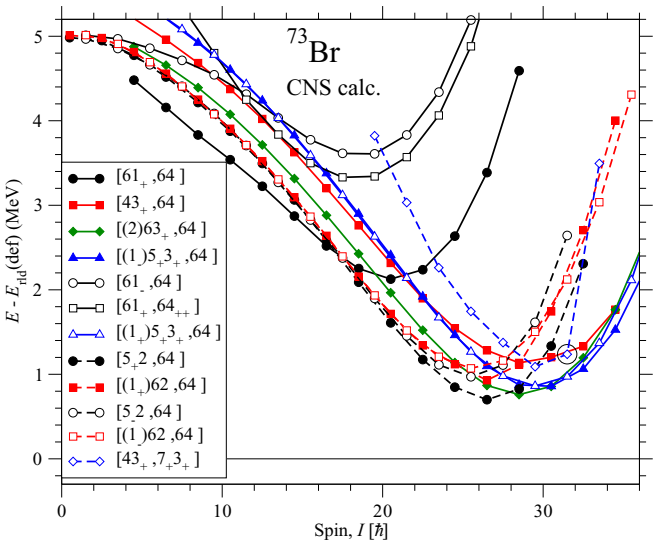

FIG. 8. Calculated low-lying configurations in ^{73}Br; energy is relative to the rotating liquid drop energy. The close-to-prolate minimum moving towards $\gamma = 60^\circ$ has been followed. Positive parity bands are drawn with full lines and negative parity with dashed lines. Closed symbols are used for signature $\alpha = 1/2$ and open symbols for $\alpha = -1/2$. The same convention is used in Figs. 9 and 11.

A subscript "+" or "−" is often added to odd occupation numbers to define the signature, $\alpha = 1/2$ or $-1/2$, respectively. In a few configurations p_0 protons are excited from $f_{7/2}$ orbitals, which is shown as $[(p_0)p_1p_2, n_1n_2]$. A shorthand notation $[p_2, n_2]$ or $[(p_0)p_2, n_2]$ is sometimes used in the text.

For the present calculations, experiment and calculation results are compared on an absolute scale using a reference energy which is also based on the LSD model [31]. The transitional quadrupole moments Q_t are calculated from the formula [37]

$$Q_t = \sqrt{\frac{8}{3}}|Q_{22}(\hat{x})| \tag{6}$$

with $Q_{22} = \sqrt{\frac{3}{2}}(y^2 - z^2)$, where the radius parameter is chosen as $r_0 = 1.2$ fm. This formula has been used, e.g., to calculate Q_t for the ultrahigh spin bands in the region around ^{158}Er [38,39].

We have identified energetically favorable configurations and observed that for low spins, say, up to $I \approx 12\hbar$, the potential energy minimum is stabilized at ($\varepsilon_2 \approx 0.4$ and $\gamma \approx -60^\circ$). Thus, collective oblate shape prevails at lower angular momentum. In contrast, as the spin increases and I approaches the highest spin in valence space configurations, $I_{\max} \approx 30\hbar$, near prolate shapes become yrast. A few noncollective configurations with ($\varepsilon_2 \approx 0.4$ and $\gamma = 60^\circ$) are calculated as yrast for some spins.

With the considerations above, the close-to-prolate minimum has been followed for low-lying configurations in ^{73}Br; see Fig. 8. The figure shows calculated excitation energy as a function of spin relative to a rotating liquid drop energy for low-lying configurations. Although in the present experiment only states up to $I \approx 20\hbar$ are observed, we will consider the full spin range reaching above $I = 30$ when comparing experiment and calculations. This is important because it is mainly for spin values $I \approx 30$ that specific features show up, which makes it possible to assign configurations to the bands in a reliable way.

The configurations considered in [13] are included in Fig. 8. However, we have noticed that configurations with proton holes in the $f_{7/2}$ shell are calculated low in energy. Interestingly, those configurations with one hole do not appear so relevant because they would show up as signature degenerate bands with $M1$'s, and no such bands are observed in ^{73}Br. However, the third configuration in Fig. 8 with two holes is quite low and might be an interpretation of band A. Furthermore, only high-spin states were considered by Plettner *et al.* Thus, the [1,4] configuration which is favored at low spin was not considered in that reference.

Based on the variation of excitation energy as a function of spin, Plettner *et al.* [10] assigned the configuration $\pi(p_{3/2}f_{5/2})^4 g_{9/2}^3 \otimes \nu(p_{3/2}f_{5/2})^6 g_{9/2}^4$ [43, 64] to band A whereas band C was described to be based on $\pi(p_{3/2}f_{5/2})^5 g_{9/2}^2 \otimes \nu(p_{3/2}f_{5/2})^6 g_{9/2}^4$ [52, 64]. The low- and medium-spin states in band B (preferably below $I = 25.5\hbar$) were found to be signature partners of band C, while the higher spin region was found to agree with the configuration $\pi(p_{3/2}f_{5/2})^4 g_{9/2}^3 \otimes \nu(p_{3/2}f_{5/2})^7 g_{9/2}^3$ [43, 73]. In the present work, new bands D and E have been observed but these bands extend to only around $12\hbar$ of spin.

It is seen that the above configurations are reproduced in our present calculation. The observed and calculated excitation energies for the configurations assigned to the bands are shown in Figs. 9(a) and 9(b) with respect to a rotating liquid drop energy, while the difference between experiment and calculations is shown in Fig. 9(c). In the high-spin region considered in [13], the [43$_+$, 64] configuration was assigned to band A. At low spin, however, band A agrees well with the [61$_+$, 64] configuration. Note that except for the highest-spin states of band B, all these bands are assigned to the same neutron configuration, $(g_{9/2})^4$.

If the low-spin region of band A is interpreted as the [1,4] configuration, the differences in Fig. 9(c) come out more are less as expected when pairing is not included, i.e., they follow a smooth trend increasing towards decreasing spin and approaching zero at high spin. The average of these differences should give a rough estimate of the pairing energy approaching 3 MeV at the ground state and coming close to zero at high spin.

The observed energies for band A indicate a band crossing at $I \approx 15$, and the calculations suggest a crossing between the [1,4] configuration and either the [3,4] or the [(2)3,4] configuration. This is thus a change from one to three $g_{9/2}$ protons, which is similar to what would be the standard interpretation in the paired formalism, i.e., an alignment of two $g_{9/2}$ protons. The present calculations do also suggest that two $f_{7/2}$ holes might be formed. However, the configuration change might then be too large and the calculated energy difference between the [3,4] and [(2)3,4] configurations is clearly uncertain within 0.5–1.0 MeV or even more.

Our work mainly concentrates on lifetime measurements of states in various bands of ^{73}Br. Hence, having assigned

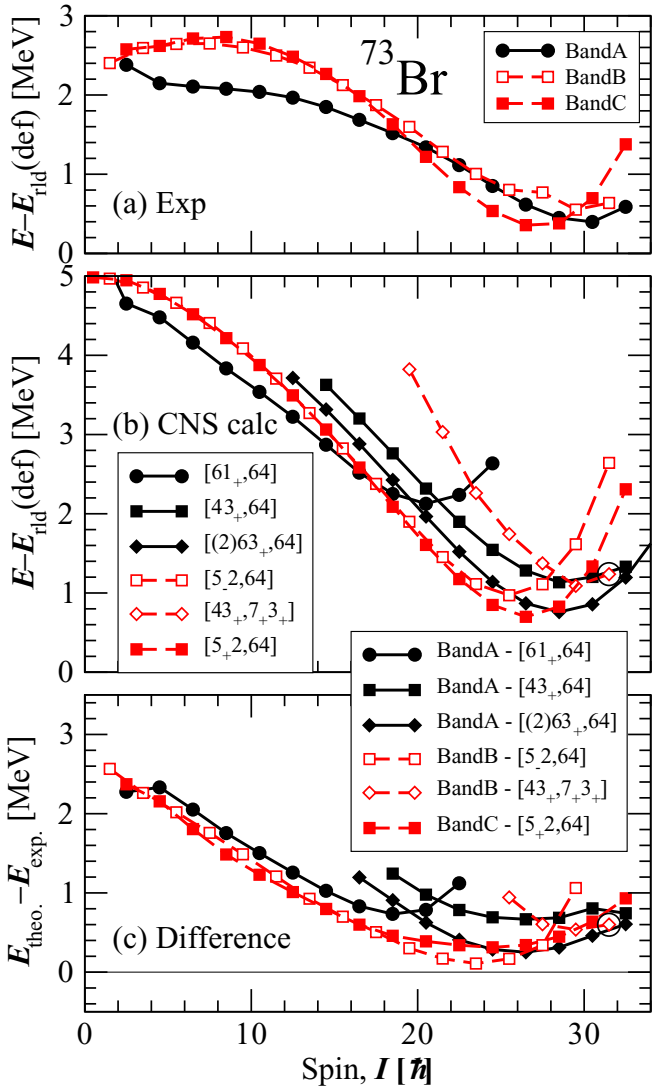

FIG. 9. Comparison between experiment and calculations. The calculated energies are obtained as discussed in the text for Fig. 8.

configurations to the observed bands depending upon comparison of excitation energy with spin, we will now compare the calculated quadrupole moments of the bands with the observed values. The quadrupole moments are calculated from the shape of the nucleus according to Eq. (6). Indeed, to a very rough estimate, Q_t is proportional to the distance from the noncollective axis, $\gamma = 60^\circ$ and -120°. Therefore, it is important to have a general understanding of the deformation for different configurations and how it develops with spin. We can then refer to Fig. 6 in Ref. [13] where deformation trajectories are drawn for the close-to-prolate minima. From this figure, it is evident that, for fixed configurations, the shape develops towards the noncollective $\gamma = 60^\circ$ axis with increasing spin, i.e., Q_t will decrease with increasing spin. Furthermore, the deformation will in general increase with more particles + holes outside closed shells, i.e., for the valence space configurations of ^{73}Br, deformation will increase with the number of particles excited across $Z = 40$ and $N = 40$ and then of course also with the number of protons excited from the $f_{7/2}$ shell. Another view of how the deformation develops is provided in Fig. 10, where total energy surfaces for the $[43_+, 64]$ configuration are drawn at different spin values. For this configuration, the close-to-prolate minimum is lowest in energy. For spin values up to $I \approx 25$, this minimum is calculated at $\gamma \approx -15^\circ$. For several other configurations, the corresponding minimum is calculated at $\gamma \approx 0^\circ$; see Fig. 6 in Ref. [13]. Note also that for the $[43_+, 64]$ configuration in Fig. 10, the close to oblate minimum at $\gamma \approx -45^\circ$ is only slighter higher in energy for spin values up to $I \approx 20$. Indeed, as mentioned above, for some other configurations, the close-to-oblate minimum is lowest in energy for low spin values. Because of this low energy and also because of the strong coupling character of bands D and E, it seems plausible that these bands are formed in this close-to-oblate minimum.

With increasing spin for the $[43_+, 64]$ configuration in Fig. 10, the close-to-prolate minimum becomes lower in energy and it dominates the energy surface for $I > 20^\circ$. Note, however, that even when the maximum spin in the configuration is reached, $I_{max} = 34.5$, the minimum is far from the noncollective axis at $\gamma = 60^\circ$. The maximum spin is easily calculated because either four or six particles in pf orbitals will at most contribute with $6\hbar$, while three or four particles in $g_{9/2}$ orbitals will have a maximum spin of $10.5\hbar$ and $12\hbar$, respectively. The nontermination of this [3,4] and other collective configurations is in line with the nontermination phenomenon discussed for ^{74}Kr in Ref. [40]. In ^{73}Br, it appears to be only configurations with at most three $g_{9/2}$ neutrons which are calculated to terminate, as exemplified by the $[43_+, 7_+3_+]$ configuration which is assigned to the highest spin states of band B.

The Q_t values calculated from the shapes of the configurations in Fig. 9 are shown in Fig. 7. These should thus be compared with the measured values. From the figure it is seen that, while the excitation energy of $[61_+, 64]$ agrees well with the experimental results at lower frequency, the quadrupole moment of this configuration matches well at higher frequencies. In contrast, the quadrupole moments of $[43_+, 64]$ and $[(2)63_+, 64]$ are higher than $[61_+, 64]$ by approximately one eb, which is close to the observed values at lower frequency. For negative parity, it is seen that for both bands B and C the average of the experimental values of Q_t comes quite close to the predictions of the theoretical calculations. However, in all the above situations, the calculated Q_t decreases smoothly with frequency whereas the experimental Q_t drops drastically. As discussed above, these bands approach their I_{max} values but they are rather far from any real termination, which means that the quadrupole moments decrease smoothly but remain relatively large, as seen in Fig. 7. It is instructive to compare with the $A = 110$ region, where experimental and calculated values of Q_t agree reasonably well [41]. Indeed, even though the bands in the $A = 110$ region appear to reach termination, the decrease of Q_t with spin is still rather gentle, except very close to termination, and less drastic than the values observed in the present case for ^{73}Br. Thus, the present values measured for Q_t are not really understood and it appears difficult to use them for configuration assignments or for predictions about termination or nontermination of these bands.

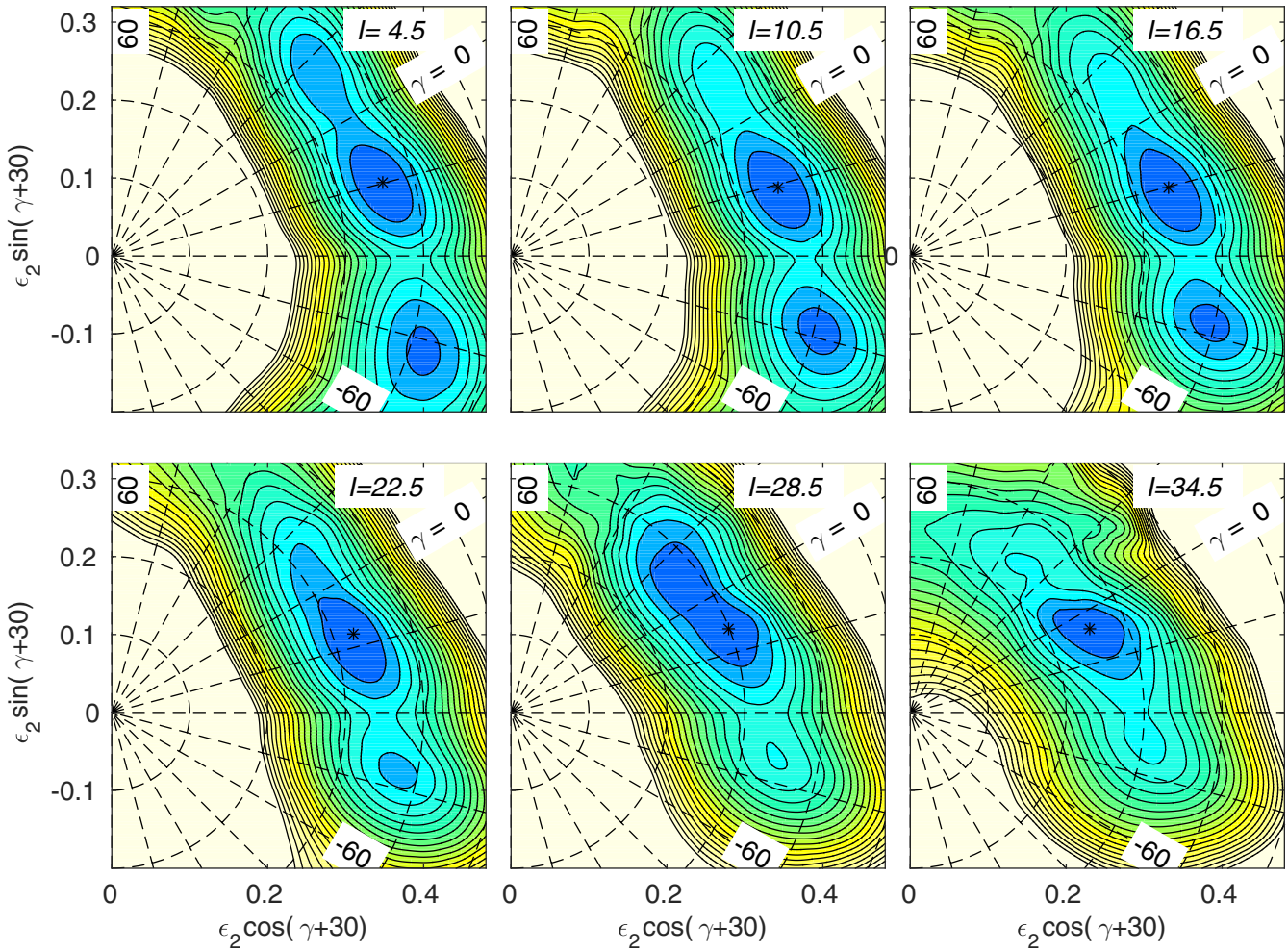

FIG. 10. Total energy surfaces for the $[43_+, 64]$ configuration of ^{73}Br. The contour line separation is 0.25 MeV.

One could also ask if the bands are approaching some band-crossing with low $B(E2)$'s in the crossing region. However, there is no real crossing in the negative parity bands, and also in the positive parity band the suggested crossing appears very soft and very smooth. The smooth character of the crossing is underlined in Fig. 11 where the observed and calculated bands are compared in I vs E_γ plots. There is a surprisingly large agreement between the paired calculations and experiment.

Looking first at band C which is assigned to the same configuration in its full range, the spin is some $3\hbar$ smaller in experiment than in calculations at low spin, suggesting that pairing is hindering the alignment of especially the high-j ($g_{9/2}$) particles at low spin. However, a very smooth transition is seen in the $I = 15$–20 spin range, so that experiment and calculations essentially coincide at high spin. The smooth transition suggests that the $B(E(2)$ values should remain reasonably smooth and large in the full spin range. The situation is similar in the other bands except for the configuration change at $I \approx 28$ in band B, which is however far outside the spin range where Q_t has been measured. At lower spins, however, there is a smooth configuration change at $I \approx 20$ also in bands A and B, where the spin is some $3\hbar$ smaller in experiment than in calculations at low spin while experiment and calculations are close to overlapping at high spin. Observe also that the agreement for band A would be very similar if the [(2)63,64] assignment at high spin would be replaced by the [43,64] configuration. We may also note that the difference between calculations and experiment is very similar for all three bands suggesting that also band A might be assigned to the same configuration, [(2)3,4] or [3,4], in its full spin range. This would agree with the large values measured for Q_t at low spin.

It is also interesting to consider the $\mathcal{J}^{(2)}$ values for the observed bands as drawn in Fig. 4(a) of Ref. [13]. We note that some rather small bumps are seen for all three bands, but these bumps show up at different frequencies, indicating that they cannot be understood as typical paired crossings within the high-j $g_{9/2}$ particles. In sumary, the nucleus ^{73}Br sees a general agreement between various observed and calculated results except for Q_t values where disagreement is seen. That might leave the question to be addressed on a broader scale which would involve minimizing uncertainties in the measurements as well as developing more reliable theoretical models or possibly tuning the parameters of the present calculations.

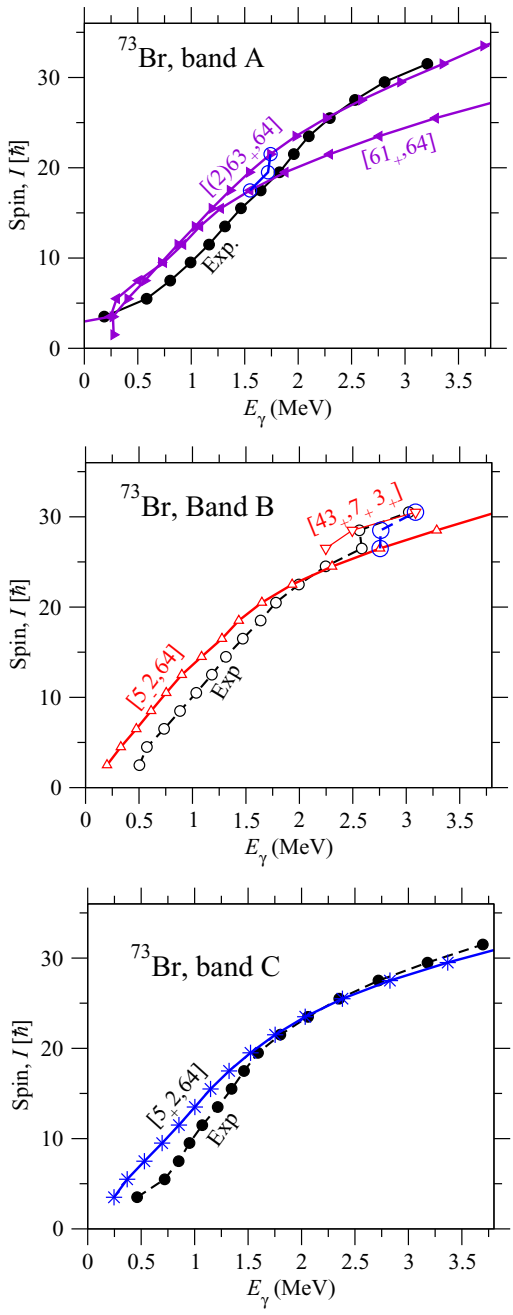

FIG. 11. Comparison between observed bands and configurations assigned to them in I vs E_γ plots. At configuration crossings, the configurations are followed beyond the crossings, while the large open circles shows the E_γ's if the lowest energies are followed through the crossings. A feature of this comparison is that it is not sensitive to excitation energies and thus is more independent of parameters. This is so because the main result of a parameter change is to change the relative energies of the different configurations.

D. TRS Calculations

The structural features of the transitional nucleus, ^{73}Br, in the $A \approx 70$ region arise due to pairing and Coriolis interactions between the individual sectors of the nucleus (protons and neutrons). Due to the presence of protons and neutrons in the high-j $g_{9/2}$ orbitals, shape coexistence and/or

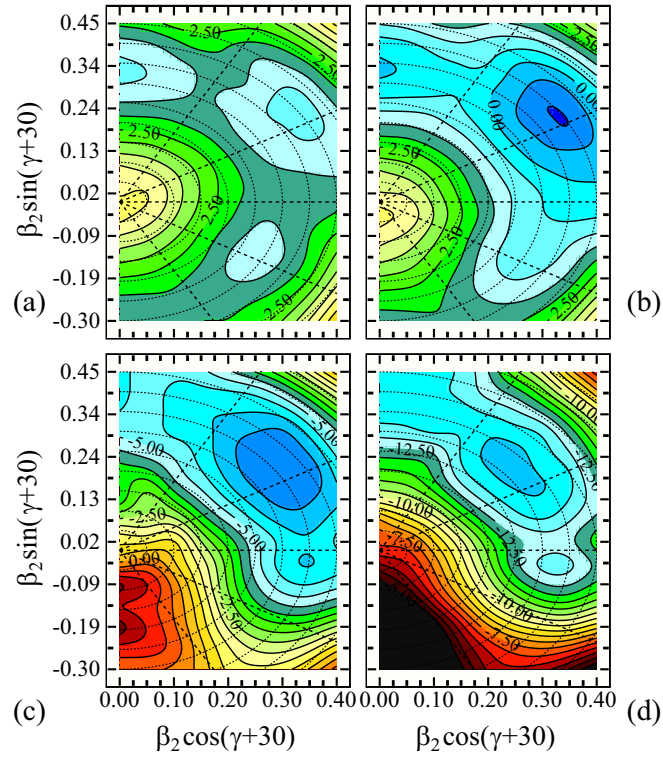

FIG. 12. Contour plots having 0.250 MeV energy difference between two consecutive contours of the TRS calculations for the positive parity quadrupole band A in ^{73}Br. The rotational frequencies ($\hbar\omega$) for the calculations are (a) 0.200 MeV, (b) 0.400 MeV, (c) 0.800 MeV, and (d) 1.100 MeV.

shape evolution becomes possible in the ^{73}Br nucleus. Five quadrupole bands having $E2$ structures have been observed in the excitation spectrum of the ^{73}Br nucleus. Among them, three positive parity quadrupole bands are generated above the $5/2^+$, $9/2^+$ and $11/2^+$ excited states in ^{73}Br. Two negative parity quadrupole bands (B and C) are observed above the $3/2^-$ and $5/2^-$ states. The CNS calculations, as described in the previous section, have been used to assign the configuration $\pi(p_{3/2}f_{5/2})^4 g_{9/2}^3 \otimes \nu(p_{3/2}f_{5/2})^6 g_{9/2}^4$ to band A and the configuration $\pi(p_{3/2}f_{5/2})^5 g_{9/2}^2 \otimes \nu(p_{3/2}f_{5/2})^6 g_{9/2}^4$ along with its signature partner to spin values below $28\hbar$ for bands C and B, respectively.

The intrinsic structure of these bands have been investigated using the total Routhian surface (TRS) calculations in the framework of the cranked shell model. The TRS, including Strutinsky shell correction, was calculated in a β_2-γ mesh for the bands of ^{73}Br. These calculations were performed for various values of rotational frequency $\hbar\omega$, and at each value of β_2-γ the total energy was minimized with respect to the hexadecouple deformation β_4.

To understand the shape of the ^{73}Br nucleus associated with the assigned configuration of quadrupole bands A (positive parity), B, and C (negative parity), the total Routhian surface (TRS) calculations [24,42] were performed with the positive ($\alpha = +1/2$), negative ($\alpha = -1/2$), and positive ($\alpha = +1/2$) signatures, respectively, in compliance with the

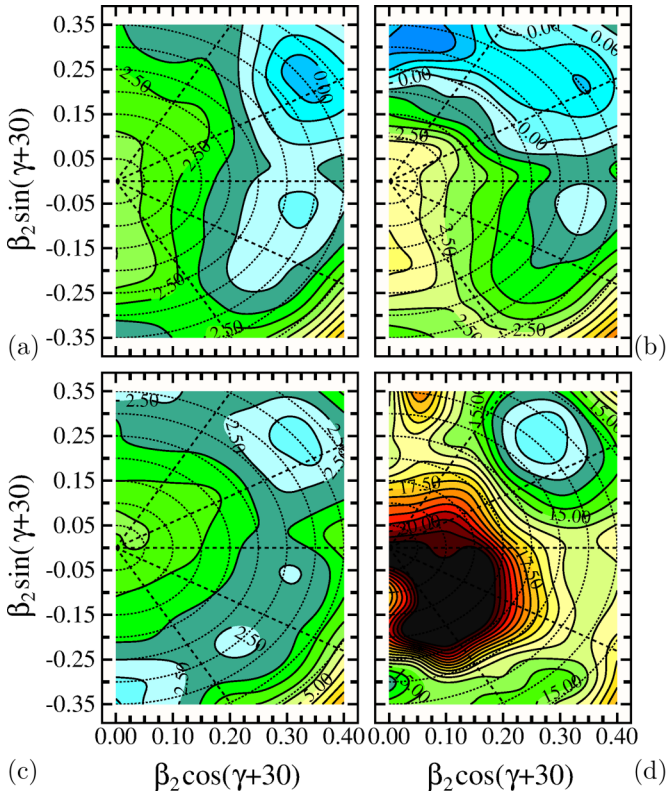

FIG. 13. Contour plots having 0.250 MeV energy difference between two consecutive contours of the TRS calculations for the negative parity quadrupole bands B [(a) and (b)] and C [(c) and (d)] in ^{73}Br. The rotational frequencies ($\hbar\omega$) for the calculations are (a) 0.400 MeV, (b) 0.800 MeV, (c) 0.400 MeV, and (d) 1.100 MeV.

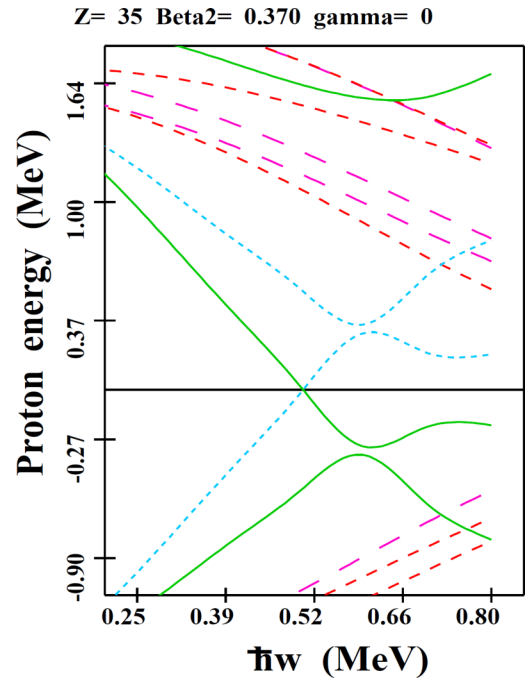

FIG. 14. Calculated quasiproton energy levels for $Z = 35$ corresponding to the ^{73}Br nucleus. Positive parity, positive and negative signature, and negative parity positive and negative signature orbitals are denoted by green, blue, red, and magenta colors, respectively.

experimentally observed spins. The contour plots of the TRS calculations of the above mentioned configurations for the positive and negative parity structures are presented in Figs. 12 and 13. These calculations exhibit that the quadrupole bands A and C favor prolate deformed shape ($\gamma \approx 0^\circ$) throughout the observed spin and frequency region [Figs. 12, 13(c), and 13(d)] in agreement with the CNS calculations, as detailed in the previous section. The signature partner band B favors the prolate deformation ($\gamma \approx 0^\circ$) at low frequencies but there is a sudden transition to noncollective oblate shape ($\gamma \approx 50^\circ$) as the most favored one at higher rotational frequencies [Figs. 13(a) and 13(b)]. Such a transition can be associated with the rotation alignment of the nucleons, indicating the termination of band B. The intrinsic shape of the nucleus associated with these quadrupole bands has been explored by calculating the quadrupole moment Q_t from the minimized β_2 and γ values as

$$Q_t = \frac{3}{\sqrt{5\pi}} ZR^2\beta_2(1 + 0.16\beta_2)\frac{\cos(\gamma + 30^\circ)}{\cos 30^\circ} \qquad (7)$$

and comparing with the experimentally measured values at different rotational frequencies. Here, β_2 and γ are the deformation parameters whereas Z and R are the proton number and the radius of the nucleus of interest, ^{73}Br, respectively.

The measured values of Q_t for the positive parity band A as well as the negative parity bands B and C are compared with the calculated Q_t values in Fig. 7. The TRS calculations predict a slower decreasing trend for the Q_t values with increasing frequency for all the three bands compared to that in the experimental data. In general, the calculated values underpredict the experimental results at the lower frequencies for all three bands. The measured Q_t values for higher frequencies in bands A, B, and C are well reproduced with TRS results, except for the $33/2^-$ state in band C, where the calculation is higher than the data.

It was suggested above that the intrinsic character of the low-spin band structures D and E corresponds to oblate shape. Such positive parity, low-spin band structures have been observed in the neighboring ^{75}Br [8] and ^{77}Br nuclei [9]. The structure of the corresponding bands in ^{75}Br and ^{77}Br originate from a quasiproton occupation of a high-K oblate orbital arising from the $g_{9/2}$ spherical shell. Indeed, such an oblate minimum (secondary minimum) has been observed at low ω ($\approx$0.200 MeV), which becomes energetically unfavorable at higher frequencies, as is evident from Figs. 10 and 12. This in fact explains the observed low and medium spin states of the band D well. The quadrupole band E may be a signature partner of the band D.

It is evident from the plot Routhians against the rotational frequency ($\hbar\omega$), as shown in Fig. 14, that there is a first band crossing at a frequency of $\approx$0.60 MeV. To improve the understanding of band crossing and shape evolution of positive parity bands D and E, TRS calculations were performed with constant deformation parameter and frequency. The variation of γ from -60° to 60° for both quasineutron and quasiproton energy with constant deformation $(\beta_2, \beta_4) = (0.37, -0.01)$

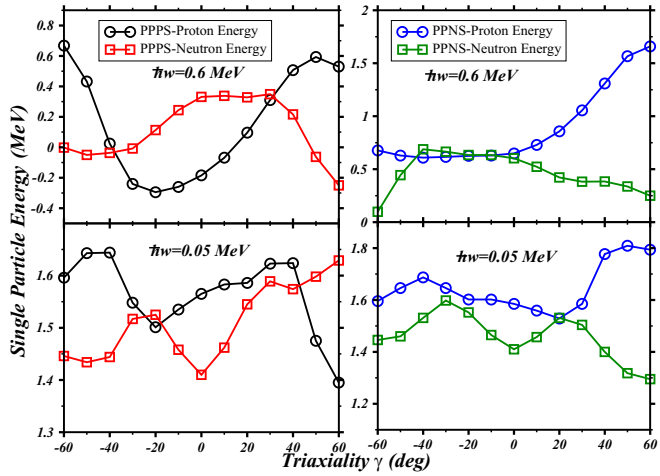

FIG. 15. Calculated single-particle energy for the positive parity positive and negative signature bands as a function of the triaxiality parameter γ for the fixed quadrupole and hexadecapole deformation parameters $(\beta_2, \beta_4) = (0.37, -0.01)$ with two different frequencies, 0.05 and 0.6 MeV respectively.

and frequency (0.05 and 0.6 MeV) is shown in Fig. 15. In ^{73}Br, the $\pi g_{9/2}$ orbital is the most crucial one to create a shape driving force. An oblate-like deformation ($\gamma = 60^\circ$) has been predicted at a low frequency of 0.05 MeV, which becomes prolate-like ($-20^\circ < \gamma < 0^\circ$) after the band crossing for both positive and negative signature positive parity bands D and E.

V. SUMMARY

High-spin states in the ^{73}Br nucleus have been studied via the ^{50}Cr(^{28}Si, αp)^{73}Br reaction. Seventeen new transitions consisting of two $\Delta I = 2$ bands have been identified for the first time. The transitional quadrupole moments have been extracted for seventeen states from measured lifetimes for three strongly populated bands of ^{73}Br by Doppler broadened line shape and the DSAM technique. The gradual decrease in the transitional quadrupole moment for positive and negative parity bands suggests the loss of collectivity with increasing spin. The reported quadrupole moments in Ref. [15] have large uncertainty and the values do not reveal a smooth trend with the variation of spin. However, the present measurements include the quadrupole moments up to high-spin states to establish the band termination phenomenon, as previously discussed [13]. The identification of interconnecting transitions between yrast negative and positive parity bands along with measured $B(E1)/B(E2)$ ratio and enhanced $B(E1)$ transition strength indicate the existence of octupole correlations in ^{73}Br. The experimental results are in fair agreement with the cranked Nilsson-Strutinsky (CNS) and total Routhian surface (TRS) calculations.

ACKNOWLEDGMENTS

The authors acknowledge the joint effort of the IUAC, New Delhi, TIFR, Mumbai, and IUC-DAEF and SINP, Kolkata, in establishing the INGA clover array, and thank the Department of Science and Technology, Government of India, for providing funds for the INGA project (No. IR/S2/PF-03/2003-I). The authors are grateful to Dr. R. Raut, UGC-DAE-CSR, Kolkata, for discussions and his help with the LINESHAPE program. The authors thank the Pelletron staff for smooth functioning of the accelerator. Financial support from the IUAC project (UFR-55313) is gratefully acknowledged.

[1] A. V. Afanasjev, D. B. Fossan, G. J. Lane, and I. Ragnarsson, Phys. Rep. **322**, 1 (1999).
[2] P. O. Tjom, R. M. Diamond, J. C. Bacelar, E. M. Beck, M. A. Deleplanque, J. E. Draper, and F. S. Stephens, Phys. Rev. Lett. **55**, 2405 (1985).
[3] J. J. Valiente-Dobon *et al.*, Phys. Rev. C **77**, 024312 (2008).
[4] T. Trivedi *et al.*, Phys. Rev. C **80**, 047302 (2009).
[5] R. Loritz *et al.*, Eur. Phys. J. A **6**, 257 (1999).
[6] R. Palit, H. C. Jain, P. K. Joshi, J. A. Sheikh, and Y. Sun, Phys. Rev. C **63**, 024313 (2001).
[7] M. K. Raju *et al.*, Phys. Rev. C **92**, 064324 (2015).
[8] G. Mukherjee *et al.*, Nucl. Phys. A **829**, 137 (2009).
[9] G. N. Sylvan *et al.*, Phys. Rev. C **48**, 2252 (1993).
[10] C. Plettner *et al.*, Phys. Rev. Lett. **85**, 2454 (2000).
[11] C. D. O'Leary *et al.*, Phys. Rev. C **69**, 034316 (2004).
[12] J. Doring, J. W. Holcomb, T. D. Johnson, M. A. Riley, S. L. Tabor, P. C. Womble, and G. Winter, Phys. Rev. C **47**, 2560 (1993).
[13] C. Plettner *et al.*, Phys. Rev. C **62**, 014313 (2000).
[14] C. Liu *et al.*, Phys. Rev. Lett. **116**, 112501 (2016).
[15] J. Heese, K. P. Lieb, L. Luhmann, S. Ulbig, B. Wormann, D. Alber, H. Grawe, H. Haas, and B. Spellmeyer, Phys. Rev. C **36**, 2409 (1987).
[16] S. Muralithar *et al.*, Nucl. Instrum. Methods Phys. Res., Sect. A **622**, 281 (2010).
[17] D. C. Radford, Nucl. Instrum. Methods Phys. Res. A **361**, 297 (1995)
[18] M. Piiparinen *et al.*, Nucl. Phys. A **605**, 191 (1996)
[19] K. Starosta *et al.*, Nucl. Instrum. Methods Phys. Res., Sect. A **423**, 16 (1999).
[20] T. Trivedi *et al.*, Phys. Rev. C **85**, 014327 (2012).
[21] R. A. Haring-Kaye *et al.*, Phys. Rev. C **92**, 044325 (2015)
[22] J. C. Wells and N. R. Johnson, Oak Ridge National Laboratory Report No. ORNL-6689, 1991 (unpublished), p. 44.
[23] L. C. Northcliffe and R. F. Schilling, At. Data Nucl. Data Tables **7**, 233 (1970)
[24] S. Rajbanshi *et al.*, Phys. Rev. C **89**, 014315 (2014)
[25] R. P. Singh *et al.*, Pramana J. Phys. **87**, 7 (2016).
[26] F. James and M. Roos, Comput. Phys. Commun. **10**, 343 (1975).
[27] P. Mason *et al.*, Phys. Rev. C **72**, 064315 (2005).
[28] S. J. Zhu *et al.*, Phys. Rev. C **85**, 014330 (2012).
[29] H. J. Li *et al.*, Phys. Rev. C **86**, 067302 (2012)
[30] K. Selvakumar *et al.*, Phys. Rev. C **92**, 064307 (2015)
[31] B. G. Carlsson and I. Ragnarsson, Phys. Rev. C **74**, 011302(R) (2006).

[32] T. Bengtsson and I. Ragnarsson, Nucl. Phys. A **436**, 14 (1985).
[33] S. G. Nilsson and I. Ragnarsson, *Shapes and Shells in Nuclear Structure* (Cambridge University Press, Cambridge, 2005).
[34] G. Andersson *et al.*, Nucl. Phys. A **268**, 205 (1976).
[35] V. M. Strutinsky, Nucl. Phys. A **122**, 1 (1968).
[36] K. Pomorski and J. Dudek, Phys. Rev. C **67**, 044316 (2003).
[37] A. Juodagalvis, I. Ragnarsson, and S. Åberg, Phys. Lett. B **477**, 66 (2000).
[38] X. Wang *et al.*, Phys. Lett. B **702**, 127 (2011).
[39] M. Matev, A. V. Afanasjev, J. Dobaczewski, G. A. Lalazissis, and W. Nazarewicz, Phys. Rev. C **76**, 034304 (2007).
[40] J. J. Valiente-Dobón, T. Steinhardt, C. E. Svensson, A. V. Afanasjev, I. Ragnarsson, C. Andreoiu, R. A. E. Austin, M. P. Carpenter, D. Dashdorj, G. de Angelis, F. Dönau, J. Eberth, E. Farnea, S. J. Freeman, A. Gadea, P. E. Garrett, A. Görgen, G. F. Grinyer, B. Hyland, D. Jenkins, F. Johnston-Theasby, P. Joshi, A. Jungclaus, K. P. Lieb, A. O. Macchiavelli, E. F. Moore, G. Mukherjee, D. R. Napoli, A. A. Phillips, C. Plettner, W. Reviol, D. Sarantites, H. Schnare, M. A. Schumaker, R. Schwengner, D. Seweryniak, M. B. Smith, I. Stefanescu, O. Thelen, and R. Wadsworth, Phys. Rev. Lett. **95**, 232501 (2005).
[41] R. Wadsworth *et al.*, Phys. Rev. Lett. **80**, 1174 (1998).
[42] S. Rajbanshi *et al.*, Phys. Rev. C **94**, 044318 (2016).